ELSEVIER

Journal of Magnetism and Magnetic Materials 138 (1994) 319–328

Journal of magnetism and magnetic materials

Frequency dispersion of permeability in ferrite composite materials

T. Nakamura [a,*], T. Tsutaoka [b], K. Hatakeyama [c]

[a] *R&D Division, Toda Kogyo Corporation, Funairi-minami, Naka-ku, Hiroshima 730, Japan*

[b] *Physics Laboratory, Faculty of School Education, Hiroshima University, Shinonome, Minami-ku, Hiroshima 734, Japan*

[c] *Resources & Environment Protection Research Laboratories, NEC Corporation, Miyazaki, Miyamae-ku, Kawasaki, Kanagawa 213, Japan*

Received 13 April 1993; in final revised form 24 May 1994

Abstract

Permeability spectra of Ni–Zn ferrite composite materials, prepared by mixing the ferrite particles with EVA resin, have been studied. In the sintered ferrite (volume fraction 1.0), the spin resonance is around 9 MHz and the static permeability about 1400. As the ferrite content decreases (composite materials), the static susceptibility of the spin component decreases and the spin resonance frequency shifts higher. The real part of the permeability in the ferrite composite materials becomes larger than that of the sintered ferrite in the rf frequency region. These features have been analyzed using the magnetic circuit model. The application of Snoek's limit extended to ferrite composite materials is also proposed.

1. Introduction

Ferrites have frequency-dependent permittivities and permeabilities. For polycrystalline ferrites, the permittivity is generally attributed to the space charges in the grain boundary, while the permeability is related to the magnetizing mechanisms: the spin rotation and domain wall motion. There have been many studies of the permeability and permittivity of polycrystalline ferrites [1–5].

Ferrite composite materials, prepared by mixing ferrite particles with appropriate amounts of resin, have also been the subject of considerable interest in recent years from the viewpoint of hybridized properties of host materials and ferrite. The permeability values and their frequency dependence can be controlled by the fabrication process of the ferrite composite materials. The permeability in ferrite composite materials has been generally estimated using the semi-empirical logarithmic law [6], but this law is inadequate to explain the frequency dependence, which is important for practical device designs [7–9]. The permeability values of composite materials are smaller than those expected from the logarithmic law.

Recently, Grimes and Grimes [10–12] calculated the effective permeability and permittivity spectra of the composite, and/or polycrystalline materials using the Clausius–Mossotti relation. They treated a regular or random array of identical spherical particles and calculated the interparticle interaction with the multipolar field expansion. This effective medium theory is a useful method for the estimation of the permeability spectra. However, some parameters used in their calculation model are complicated and it is

* Corresponding author.

SSDI 0304-8853(94)00418-Q

difficult to make relations between their parameters and the practical material characters such as volume loading and character of dispersed particles.

Doyle and Jacobs [13,14] considered the permittivity of the metal–insulator composites, in which the conducting particles are dispersed in the insulating matrix. They showed that the large enhancement of the permittivity occurred at high volume loading of the conducting particle and the permittivity becomes higher than that predicted by the Clausius–Mossotti approximation. The dielectric anomaly is attributed to the percolation problem and the formation of the conduction path with the contact of the particles. Their metal–insulator composite model was started from that with the low volume loading. On the other hand, the ferrite composite can be regarded as a sintered ferrite which has many magnetic gaps. The magnetic gaps introduced into the sintered ferrite play an important role in reducing the permeability below that expected by the logarithmic law. How and Vittoria [15] treated the composite consisting of a regular array of magnetic particles and calculated the permeability taking into account the demagnetizing energy. They deduced the effect of shape anisotropy and particle configuration on the demagnetizing factor.

Johnson and Visser proposed a simple model for the magnetic gaps in polycrystalline ferrite [16]. They considered that the ferrite grains are surrounded by nonmagnetic grain boundary layers with large magnetic resistivity. They called this model a 'coherent model'. From an analysis of the permeability using this model, they estimated the thickness of the nonmagnetic grain boundary layer as about 1 nm; this size remains constant when the size of the ferrite grain changes. We have studied the frequency dispersion of the permeability for Ni–Zn ferrite composite concerning this coherent model and have proposed a simple model for the frequency dispersion of permeability of the ferrite composite materials [17,18]. This model is based on the relaxation-type spin resonance formulation combined with the magnetic circuit model, where the ferrite composite materials are considered to have the coherent structure of the ferrite particles and highly resistive host resin.

In the present work, we have made more detailed studies of the frequency dispersion of the permeability for Ni–Zn ferrite composite materials in the rf frequency region. This paper discusses a quantitative treatment of spin permeability in the rf frequency region, and mechanisms for the permeability variation with the ferrite particle content in ferrite composite materials. The paper also shows how our model can be applied to the design of high-frequency devices such as electromagnetic wave absorbers.

2. Experimental procedures

2.1. Sample preparation

Ni–Zn ferrite particles, with average diameters of 0.2–1.5 mm, were prepared by mechanical granulation of the ferrite powders and by sintering in air at 1150°C and slowly cooling to room temperature. The ferrite particles had a lattice constant $a = 8.402$ Å, Curie temperature $T_C = 380$ K, and composition $Ni_{0.24}Zn_{0.65}Cu_{0.07}Fe_{2.04}O_4$. The ferrite composite materials were made by mixing the ferrite particles with appropriate amounts of EVA (ethylene–vinyl–acetate polymer) resin and pressing the mixture into a ring form. The inner and outer diameters were 17 and 38.5 mm, respectively. Several samples with thickness 5–10 mm were prepared. Since both the ferrite particle diameter and the ferrite content can be important factors in the permeability of the ferrite composite materials, two series of samples were prepared to examine the effects of the ferrite particle diameter and the ferrite content on the permeability. These were: (1) almost the same density values and different particle diameters, and (2) almost the same average particle diameters and different density values.

2.2. Permeability measurements

The complex permeability ($\mu^* = \mu' - i\mu''$) of the samples were measured by two different techniques. In the frequency range 100 kHz to 10 MHz, μ^* was obtained by measuring the inductance and the resistance differences between a toroidal coil wound around the toroidal sample and one wound around a toroidal Teflon blank, using a low-frequency impedance analyzer (Hewlett Packard 4192A). In the frequency range 1 MHz to 1 GHz, μ^* was obtained by measuring the input impedance of samples by the

coaxial line technique with an rf-network analyzer (Hewlett Packard 8510B). The experimental error for the complex permeability is less than 5%.

3. Experimental results

Fig. 1(a) shows the variation of the real part of the permeability μ' at 100 kHz and 100 MHz with the average diameter of the ferrite particles, where the density of the composite materials was at an almost constant value of 3.7 g/cm^3. Fig. 1(b) shows the variation of μ' at 100 kHz and 100 MHz with the density of the composite materials, where the average diameter of the ferrite particles was constant at 1.5 mm. These two figures indicate that the permeability depends only on the density of the composite materials, i.e. the ferrite particle content. In this study, therefore, we consider only the effects of the ferrite content.

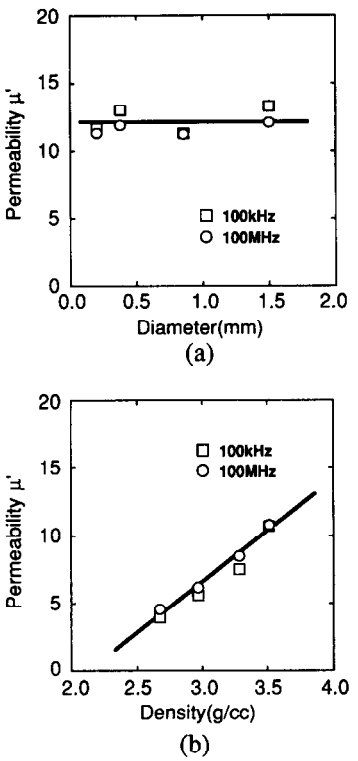

Fig. 1. Variation of the real part of the permeability μ' with average particle diameter (a), and the density of the composite materials (b). Solid lines are guides for the eyes.

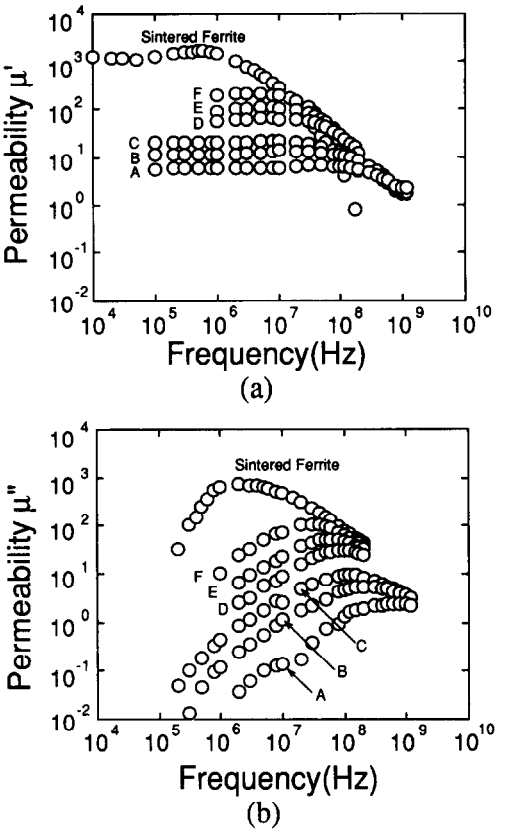

Fig. 2. Real (a) and imaginary (b) parts of permeability (μ' and μ'') for Ni–Zn ferrite composites.

The dispersion curves of complex permeability for the ferrite composite materials and the sintered ferrite are shown in Fig. 2 ((a) real part μ' and (b) imaginary part μ''). For sintered ferrite, the real part μ', which is about 1400 in the low-frequency region, begins to decrease at about 1 MHz, and reaches about 10 at 100 MHz. On the other hand, the imaginary part μ'' has a maximum of about 800 at around 1 MHz. For polycrystalline ferrites, the permeability spectrum can be described by the superposition of two components that can be attributed to two types of magnetizing processes, spin rotation and domain wall motion [3]:

$$\mu(\omega) = 1 + \chi_{\text{spin}}(\omega) + \chi_{\text{dw}}(\omega). \quad (1)$$

We assume that the spin rotation component χ_{spin} is

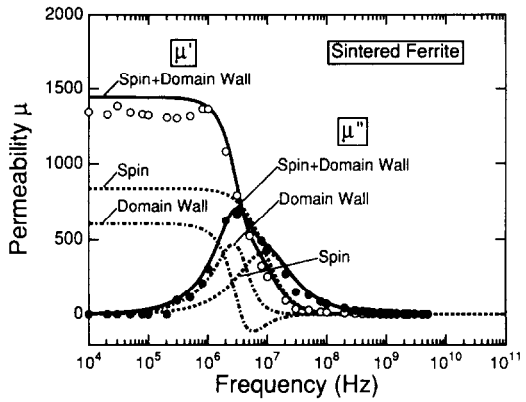

Fig. 3. Permeability spectra of a sintered ferrite. Experimental values are denoted by open circles (μ') and solid circles (μ''). Solid lines show total permeability combined with spin rotation component (broken lines) and domain wall motion component (dash-dotted lines).

relaxation type and that the domain wall component χ_{dw} is resonance type:

$$\chi_{spin}(\omega) = \frac{K_s}{1 + i(\omega/\omega^{res})}, \quad (2)$$

$$\chi_{dw}(\omega) = \frac{K_{dw}\omega_{dw}^2}{\omega_{dw}^2 - \omega^2 + i\beta\omega}, \quad (3)$$

where K_s and ω^{res} correspond to the static spin susceptibility and the spin resonance frequency, respectively, and K_{dw}, ω_{dw} and β are the static susceptibility of the domain wall motion, the domain wall resonance frequency and the damping factor for the domain wall motion, respectively. From the numerical fitting of the dispersion curve of the sintered ferrite (Fig. 2) to these equations, we obtained the set of the parameters as $K_s = 839$ and $\omega^{res} = 9.17$ MHz for the spin rotation component, and the set $K_{dw} = 603$, $\omega_{dw} = 3.62$ MHz and $\beta = 5.34$ MHz for the domain wall motion. Using Eqs. (1)–(3) with these parameters, we calculated the permeability spectrum for the sintered ferrite, which is shown in Fig. 3. Each calculated spectrum of spin rotation and domain wall motion is also shown in this figure. Good agreement between experimental dispersion and calculation curve was obtained. The complex permeability in high-frequency region above 10 MHz can be described with the spin rotation component.

The dispersion curves of μ^* for the ferrite composite materials are also shown in Fig. 2. Samples A, B and C have the ferrite particle contents of 50.0, 68.0 and 72.0 vol%, respectively. Samples D, E and F, with high ferrite contents of 95.0, 96.5 and 98.0 vol%, were prepared by cracking the sintered core and by bonding them together. In the low-frequency region, both the real and imaginary parts of μ^* decrease with decreasing ferrite content. However, in the high-frequency region (for example, about 100 MHz), the μ' of the ferrite composite is larger than that of the sintered ferrite. As the ferrite content decreases, both the shoulder frequency of μ' and the peak frequency of μ'' shift higher. The cracking of the sintered ferrite (samples D, E and F) also leads to the same type of changes in the permeability dispersion: both the real and imaginary parts of the low-frequency permeability are significantly reduced, and the peak frequency of μ'' shifts toward higher frequency. It is important that the cracked sintered ferrite shows intermediate permeability spectra between those of the sintered ferrite and composite materials.

We applied the spin resonance formulation to the ferrite composite materials, and calculated the parameters by fitting the experimental data in 100 MHz region in Fig. 2 to Eq. (2). Table 1 shows the parameters of the examined samples. It indicates that the K value decreases and the ω^{res} shifts toward higher frequency when the ferrite content decreases.

4. Model calculation

We consider the ferrite composite materials to be composed of spherical polycrystalline ferrite parti-

Table 1
Permeability dispersion parameters of Ni–Zn ferrite composites for spin resonance

Sample	ρ (g/cm^3)	Vol%	K	ω^{res} (MHz)
A	2.97	49.3	4.97	850
B	3.73	68.3	9.08	461
C	3.87	71.8	11.36	341
D	4.80 [a]	95.0	59.28	98.2
E	4.86 [a]	96.5	99.26	65.2
F	4.93 [a]	98.3	200.6	34.4
Sintered ferrite	5.10	100	839.0	9.17

[a] Density values calculated from the gap parameter.

cles surrounded by a nonmagnetic resin layer. The schematic configuration is shown in Fig. 4. The average size of the ferrite particles and the average thickness of the nonmagnetic resin layer are denoted by D and $\delta/2$, respectively. There are two magnetic resistivities: intraparticle resistivity (grain boundary) and interparticle resistivity (resin layer). Since the magnetic resistivity of the resin layer is much higher than that of the grain boundary in the ferrite particle, we can describe the magnetic circuit, that is the Ampère's integral, in the ferrite composite materials using only the resistivity of the resin layer:

$$\frac{(D+\delta)}{\mu} = \frac{D}{\mu_B} + \delta, \tag{4}$$

where μ and μ_B are the effective permeability of the ferrite composite materials and the permeability of the ferrite particle, respectively. The values of D and δ do not change with the frequency. Furthermore, the permeability of the ferrite particle is almost equal to that of the sintered ferrite. Therefore, we obtain the following equations, in which K and ω^{res} are functions of only δ/D:

$$\mu(\omega) = \frac{\mu_B(1+\delta/D)}{1+\mu_B(\delta/D)} = 1 + \frac{K}{1+i(\omega/\omega^{res})}, \tag{5}$$

$$K = \frac{K_B(1+\delta/D)}{1+K_B(\delta/D)}, \tag{6}$$

$$\omega^{res} = \omega_B^{res}(1+K_B(\delta/D)). \tag{7}$$

The ratio of δ/D is related to the density of ferrite composite materials, and increases with a decrease in density. Although the ferrite particle size and the resin layer thickness have distributions, we consider only the average values represented in Fig. 4. Assuming that the ferrite particles with uniform size are homogeneously distributed in the composite, the density of the composite ρ is given by

$$\rho = \frac{D^3\rho_f + \left[(D+\delta)^3 - D^3\right]\rho_m}{(D+\delta)^3} \tag{8}$$

where ρ_f and ρ_m are the densities of the ferrite and resin, respectively. Thus, the average value of δ/D can be estimated from the density of the composite materials using the equation:

$$\left(1+\frac{\delta}{D}\right)^3 = \frac{\rho_f - \rho_m}{\rho - \rho_m}. \tag{9}$$

We call the δ/D 'gap parameter'. Therefore, the permeability of composite materials depends only on the ferrite content in this formulation. Since the ferrite content is related solely to the density of the ferrite composite materials, as we shall see, this feature supports the experimental results.

Fig. 5 shows the variation of the dispersion parameters K and ω^{res} with the gap parameter. The open and solid circles denote K and ω^{res}, respectively. The K value decreases and the resonance frequency ω^{res} shifts to a higher-frequency range when δ/D increases. The solid lines indicate the curves calculated from Eqs. (6) and (7) using the sintered ferrite parameters. A significant correlation between experimental and theoretical values is obtained. Therefore, this allows us to evaluate quantitatively the permeability of the ferrite composite materials in the rf frequency region using our calculation

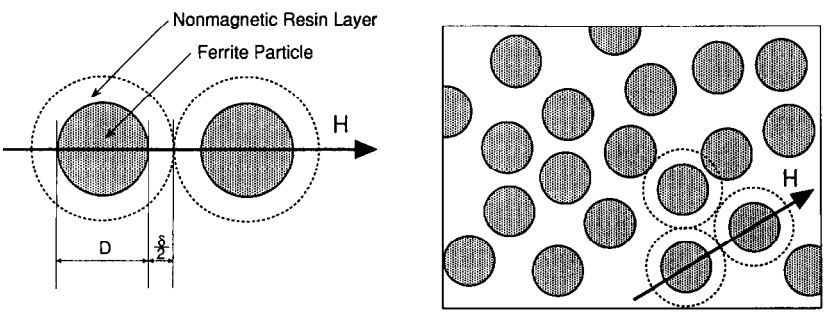

Fig. 4. Magnetic circuit model for ferrite composite materials.

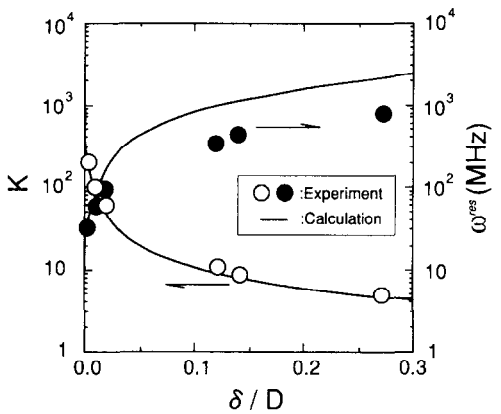

Fig. 5. Variation of the dispersion parameters (static spin susceptibility K and spin resonance frequency ω^{res}) with the gap parameter (δ/D). The solid lines denote the calculated curves using the magnetic circuit model.

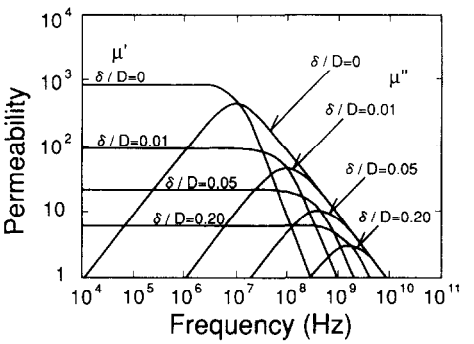

Fig. 6. Frequency dispersion curves for the spin permeability calculated using the magnetic circuit model at each gap parameter value.

model. Fig. 6 shows the calculated complex permeability curves for ferrite composite materials in various δ/D values. Both the real and imaginary parts of μ in the low-frequency region decrease when the δ/D value increases. Simultaneously, both the shoulder frequency of μ' and the peak frequency of μ'' shift toward higher frequency. In the 100 MHz region, μ'' decreases with increasing δ/D and the μ' at $\delta/D = 0.01$ is larger than that of the others.

We examine the variation of the permeability in the frequency range 50–200 MHz with the ferrite content. Fig. 7 shows the variations in the complex permeability at 50, 100, 150, and 200 MHz in the ferrite composite materials with the gap parameter. The imaginary part μ'' decreases when the ferrite content is decreased, whereas the real part μ' has a maximum value of μ'_{max} at a finite value of $(\delta/D)_c$. The maximum value μ'_{max} decreases and the critical value of $(\delta/D)_c$ increases when the frequency increases. For example, at 100 MHz, the critical value $(\delta/D)_c$ is about 0.01 and the maximum value of μ'_{max} is about 40. Using the magnetic circuit model calculation, we can expect the frequency dependence of the critical value $(\delta/D)_c$ and that of the maximum value μ'_{max}. Differentiating the real part of Eq. (5) with respect to δ/D and taking it to be zero at

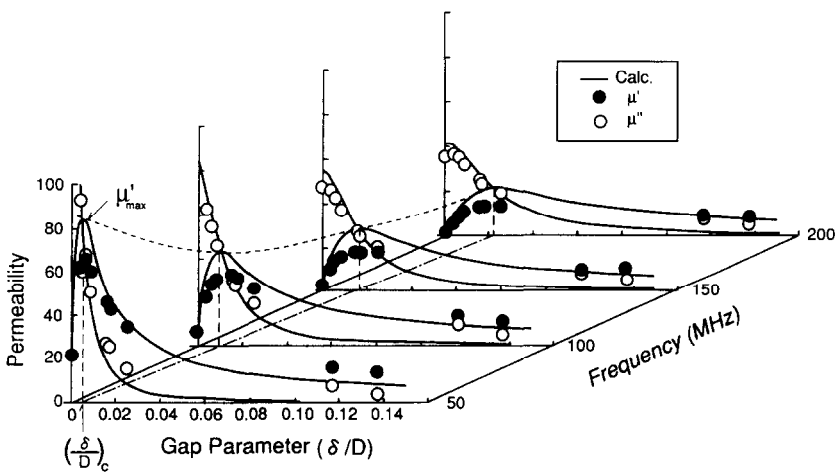

Fig. 7. Gap parameter dependence of the permeability at 50, 100, 150 and 200 MHz for the ferrite composite materials. The solid lines denote the calculated curves using the magnetic circuit model.

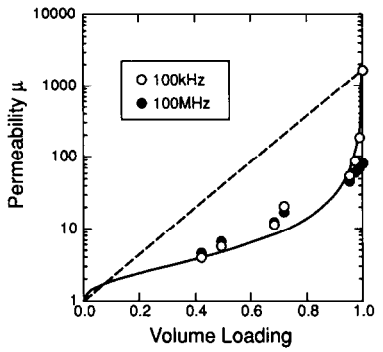

Fig. 8. Variation of the absolute value of complex permeability with volume loading. Open circles denote experimental values at 100 kHz; closed circles denote those at 100 MHz. Solid and dashed lines indicate the calculated curves for the magnetic circuit model and the logarithmic law, respectively.

$(\delta/D)_c$, the following equations are found in the frequency region of $\omega/\omega_B^{res} \ll K_B$:

$$\left(\frac{\delta}{D}\right)_c \approx \frac{1}{K_B}\left(\frac{\omega}{\omega_B^{res}} - 1\right), \tag{10}$$

$$\mu'_{max}(\omega) \approx \tfrac{1}{2}\frac{K_B \omega_B^{res}}{\omega}. \tag{11}$$

The critical value $(\delta/D)_c$ increases linearly with frequency. Eq. (11) indicates that μ'_{max} is inversely proportional to the frequency. The maximum value is determined by the product of the static susceptibility K_B and the spin resonance frequency ω_B^{res}. This relation corresponds to Snoek's limit [1]. Therefore, we consider Eq. (11) to be Snoek's limit extended to ferrite composite materials.

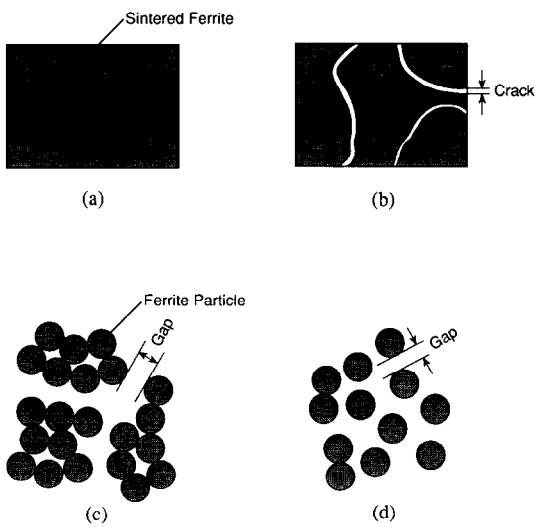

Fig. 9. Schematic configurations of sintered ferrite (a), cracked sintered ferrite (b), composite material with high ferrite content (c) and composite material with low ferrite content (d).

5. Discussion

It is meaningful to compare the permeability evaluated by the magnetic circuit model with that estimated by the logarithmic law. Fig. 8 shows the variation of the absolute value of the permeability with the volume loading of ferrite in the composite materials. The solid line denotes the permeability change obtained by the magnetic circuit model and the dashed line is obtained by the logarithmic law. Open and closed circles indicate the experimental values at 100 kHz and 100 MHz, respectively. The logarithmic law leads to an over-estimation of the permeability, and the magnetic circuit model provides the values nearly equal to the experimental values. In ferrite composite materials, a magnetic inert component is introduced that causes not only the magnetic dilution but also a cut-off of the magnetic circuit in the ferrite. Therefore, the permeability is reduced remarkably as the ferrite volume loading decreases. This feature is similar to the permittivity enhancement in metal–insulator composites [13,14].

We consider that the configuration of magnetic connection changes continuously from sintered ferrite to ferrite composite materials. The schematic configuration changes are shown in Fig. 9 for the sintered ferrite (a), the cracked sintered ferrite (b), the ferrite composite material with high volume loading (c), and with low volume loading (d). The magnetic gaps in the sintered ferrite can be negligible, so that the magnetic moment is easily aligned along an applied field. In the cracked sintered ferrite, the magnetic gaps are introduced and the magnetic poles are created at the boundary between the ferrite and the magnetic inert component in the presence of an applied field. The magnetic poles create the demagnetizing field antiparallel to the applied field. In the composite materials with high volume loading, some ferrite particles aggregate to form a magnetic cluster and the magnetic poles on the surface of the cluster

contribute the demagnetizing field. Further, low volume loading composites have magnetic particles separated individually, and the magnetic poles on each ferrite particle generate the demagnetizing field. The demagnetizing field reduces the induced magnetic moment more than that calculated from the volume loading. Therefore, the permeability in low-frequency region decreases with the configuration change from the sintered ferrite to the ferrite composite materials.

On the other hand, the spin resonance frequency ω^{res} is represented by the equation [2,3]:

$$\omega^{res} = \gamma H_a, \tag{12}$$

where H_a is the effective anisotropy field and γ is the gyromagnetic ratio. The effective anisotropy field is written by the summation of the magnetocrystalline anisotropy field and the shape anisotropy field. The former is determined by the composition and the crystal structure of the magnetic component, and the latter depends on the particle shape and the particle configuration. For the sintered ferrite, the contribution of the magnetocrystalline field is larger than that of the shape anisotropy field, since the magnetic gaps can be negligible. In the cracked sintered ferrite, the magnetic gaps break down the magnetic connection and sintered ferrite is separated into finite magnetic parts with a magnetic inert component. Therefore, the shape anisotropy field is introduced, which is equivalent to the demagnetizing field H_d induced by the rf magnetic field. The spin resonance frequency is given by

$$\omega^{res} = \gamma(H_a + H_d). \tag{13}$$

The spin resonance frequency shifts higher due to the contribution of the demagnetizing field. For the ferrite composite materials consisting of isotropic shape particles, there are some aggregates in the case of high volume loading and the particles are dispersed individually in the case of low volume loading. Since the cluster of the magnetic particles responds as a magnetic unit, the number of magnetic poles per unit volume is less than that for isolated particles. Thus, demagnetizing field increases with decreasing volume loading, and the spin resonance frequency becomes higher. As the result, the μ' can take a larger value than that of the sintered ferrite in the rf frequency region.

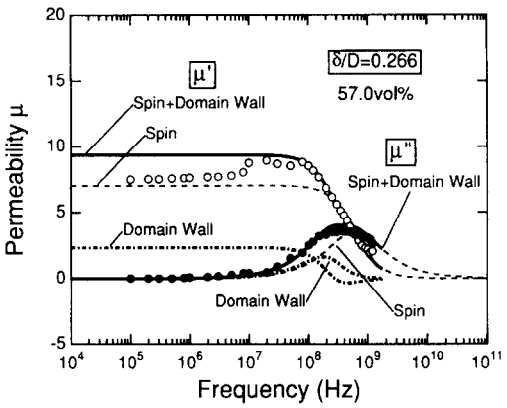

Fig. 10. Permeability spectra of a ferrite composite material. Experimental values are denoted by open circles (μ') and solid circles (μ''). Solid lines show the total permeability combined with spin rotation component (broken lines) and domain wall motion component (dash-dotted lines).

Fig. 10 shows the permeability spectra for a ferrite composite material with a 57% volume fraction of ferrite. The spin rotation component is calculated from Eqs. (5), (6) and (7). The permeability in the frequency region above 100 MHz can be reproduced only with the spin rotation component. However, the permeability spectrum in the low-frequency region below 10 MHz can not be realized by considering the contributions of both the domain wall motion and the spin rotation. This discrepancy can be regarded as the microstructure difference between the sintered ferrite and the ferrite particles in composite materials. Since the dispersion parameters of the domain wall motion are sensitive to the microstructure of the polycrystalline ferrite, the parameters obtained in the sintered ferrite cannot be applied to calculate the parameters of composite materials. Therefore, it is necessary to evaluate the microstructure both of the sintered ferrite and ferrite particles in the composite materials in order to consider the contribution of the domain wall motion. Accordingly, further investigations are needed to understand the contribution of the domain wall motion.

6. Applications

We examine the electromagnetic wave absorber using the ferrite composite materials. We can design

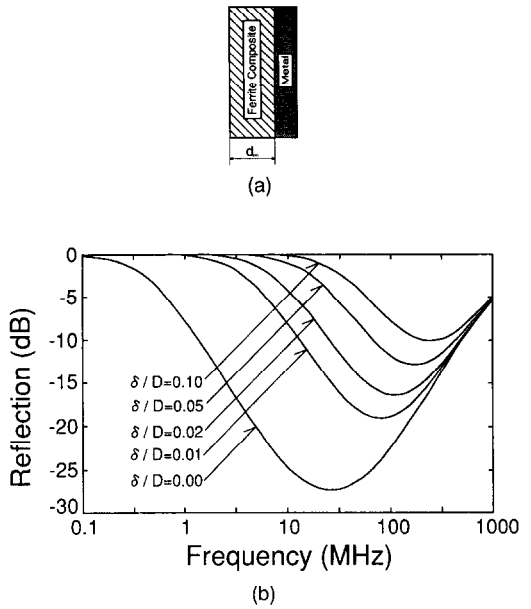

Fig. 11. Structure of a single-layer electromagnetic wave absorber (a), and the variation of the absorption characteristics with the gap parameter (b).

the single-layer electromagnetic wave absorber for the rf frequency region using these dispersion curves. The structure of the absorber is shown in Fig. 11(a). By assuming that the thickness of the absorber d_m is small enough compared with the wavelength of the incident electromagnetic wave, the input impedance $Z(\omega)$ can be calculated with the equation

$$Z(\omega) = Z_0 \mathrm{i} \frac{\omega}{c} \mu d_m = Z_0 \mathrm{i} \frac{\omega}{c} (\mu' - \mathrm{i}\mu'') d_m, \qquad (14)$$

where Z_0 is the characteristic impedance of the free space. The reflection $\Gamma(\omega)$ is shown by the equation

$$\Gamma(\omega) = \frac{Z(\omega) - Z_0}{Z(\omega) + Z_0}. \qquad (15)$$

For the sintered ferrite, it is necessary to select the thickness of the absorber d_m at about 7 mm in order to get the matching of the impedance in the 100 MHz region [18]. For a fixed thickness, the front face reflection is calculated by Eqs. (14) and (15). Fig. 11(b) shows the variation of the absorption with frequency at several gap parameters at a constant absorber thickness of 7 mm. The center frequency of the absorption shifts toward higher frequency and the maximum absorption is reduced as the gap parameter increases. These features can qualitatively reproduce the experimental data for a poorly densified ferrite ceramics absorber [19].

7. Concluding remarks

We have studied the frequency dispersion of the permeability for Ni–Zn ferrite composite materials using the spin resonance formulation combined with the magnetic circuit model. The model analysis includes the effect of the demagnetizing field and makes it clear that the permeability in the rf frequency region depends only on the volume loading of ferrite. In the ferrite composite materials, the real part of the permeability in the rf frequency region becomes larger than that of the sintered ferrite. This is attributed to the shift of the spin resonance frequency toward the higher frequency region by introducing a demagnetizing field in the ferrite composite materials. Snoek's limit can be extended to the ferrite composite materials. We can estimate the frequency dispersion of the permeability in ferrite composite materials on the basis of this model using the dispersion parameters of guest magnetic materials. We have also proposed the possibility of designing electromagnetic wave absorbers using this formulation. However, this model calculation is insufficient to evaluate the dispersion of the low-frequency permeability below about 10 MHz, even though the contribution of the domain wall motion is taken into account. This may be attributed to the difference between the domain structures of the sintered ferrite and the ferrite particles. More detailed studies of the permeability dispersion in the low-frequency region are being carried out.

Acknowledgements

The authors are grateful to Mr Yamamoto of Toda Kogyo Corporation for his help in the sample preparation, Mr Hankui of NEC Corporation for his help in the impedance measurements, and Mr Shimizu of NEC Environment Engineering Ltd and Mr Horiishi of Toda Kogyo Corporation for their encouragement during this work.

References

[1] J.L. Snoek, Physica XIV 4 (1948) 207.
[2] D. Polder and J. Smit, Rev. Mod. Phys. 25 (1953) 89.
[3] G. Rado, Rev. Mod. Phys. 25 (1953) 81.
[4] A. Globus, J. Physique Suppl. C1 (Proc. ICF-3) (1977) 1.
[5] J.P. Bouchaud and P.G. Zerah, J. Appl. Phys. 67 (1989) 5512.
[6] J.B. Birks, Proc. Phys. Soc. LX3 (1947) 282.
[7] M.J. Conen, Proc. 9th Int. Conf. on EMC (1991) 557.
[8] F. Mayer and J.P. Chaumat. Proc. 9th Int. Conf. on EMC (1991) 569.
[9] S.A. Mirtaheri, T. Mizumoto, and Y. Naito, Trans. IEICE E73 10 (1990) 1746.
[10] C.A. Grimes and D.M. Grimes, Phys. Rev. B 43 (1991) 10780.
[11] C.A. Grimes and D.M. Grimes, J. Appl. Phys. 69 (1991) 6186.
[12] C.A. Grimes, IEEE Trans. Magn. 27 (1991) 4310.
[13] W.T. Doyle and I.S. Jacobs, Phys. Rev. B 42 (1990) 9391.
[14] W.T. Doyle and I.S. Jacobs, J. Appl. Phys. 71 (1992) 3296.
[15] H. How and C. Vittoria, J. Appl. Phys. 69 (1991) 5138.
[16] M.T. Johnson and E.C. Visser, IEEE Trans. Magn. 26 (1990) 1987.
[17] S. Yamamoto, T. Nakamura, T. Tsutaoka, S. Shimizu, E. Hankui, and K. Hatakeyama, IEICE Tech. Rep. 92 156 (1992) 27 (in Japanese).
[18] T. Nakamura, S. Yamamoto, T. Tsutaoka, S. Shimizu, E. Hankui, and K. Hatakeyama, Proc. 6th Int. Conf. on Ferrites (1992) 1298.
[19] Y. Naito, Proc. Int. Conf. on Ferrites (1970) 558.
[20] C. Kittel, Phys. Rev. 73 (1948) 155.
[21] Y. Naito, Trans. IEICE B 52-B 1 (1969) 21.
[22] H.T. Hahn, J. Appl. Phys. 69 (1991) 6195.